*Structural Engineering and Mechanics, Vol. 25, No. 6 (2007) 653-674*
DOI: http://dx.doi.org/10.12989/sem.2007.25.6.653 

# Application of Hilbert-Huang transform for evaluation of vibration characteristics of plastic pipes using piezoelectric sensors

N. Cheraghi, M.J. Riley and F. Taheri†

*Department of Civil Engineering, Dalhousie University, 1360 Barrington Street, Halifax, Nova Scotia B3J 1Z1, Canada*

*(Received July 20, 2005, Accepted September 5, 2006)*

**Abstract.** This paper discusses the application of piezoelectric sensors used for evaluation of damping ratio of PVC plastics. The development of the mathematical formulation based on the Empirical Mode Decomposition for calculating the damping coefficient and natural frequency of the system is presented. A systematic experimental and analytical investigation was also carried out to demonstrate the integrity of several methods commonly used to evaluate the damping of materials based on a single degree freedom formulation. The influence of the sensors' location was also investigated. Besides the commonly used methods, a newly emerging time-frequency method, namely the Empirical Mode decomposition, is also employed. Mathematical formulations based on the Hilbert-Huang formulation, and a frequency spacing technique were also developed for establishing the natural frequency and damping ratio based on the output voltage of a single piezoelectric sensor. An experimental investigation was also conducted and the results were compared and verified with Finite Element Analysis (FEA), revealing good agreement.

**Keywords:** plastics; damping; FFT; finite analysis; Hilbert transform; frequency spacing; Empirical Mode Decomposition (EMD).

## 1. Introduction

Characterization of damping forces in a vibrating structure has long been an active and challenging area of research in structural dynamics. The demands of modern engineering have led to a steady increase in the interest in recent years. Nonetheless, in spite of a large amount of research, the fundamental understanding of structural damping still requires further exploration. A major obstacle is that in comparison to the forces related to the inertia and strain energy of the body, it is not generally clear which state variables would be the most relevant for determining the damping force. By far the most common approach is to assume the so-called "viscous damping", a linear model in which it is assumed that the instantaneous generalized velocities are the only relevant state variables that affect damping. This approach was first introduced by Rayleigh (1945) via his famous "dissipation function", in which a quadratic expression was formulated to characterize the energy dissipation rate with a symmetric matrix of coefficients, also refereed to as

† Professor, Ph.D., Corresponding author, E-mail: farid.taheri@dal.ca

the "damping matrix". A further idealization, also pointed out by Rayleigh, is to assume the damping matrix to be a linear combination of the mass and stiffness matrices.

Rayleigh was quite clear in stating that his proposed approach was solely based on mathematical convenience, because it allowed the damping matrix to be simultaneously diagonalized with the mass and stiffness matrices, thus preserving the simplicity of an uncoupled and real normal mode, as in an undamped case. Since its introduction, this method has been used extensively and is now usually referred to as the "Rayleigh damping", or the "proportional damping", or the "classical damping" method.

Imregun (1991) compared two different single-degree-of-freedom (SDOF) modal analysis techniques, as well as a global multi-degree-of freedom (MDOF) method applied to frequency response function measurements taken on a lightly damped linear structure. For the SDOF, the circle-fit and the line-fit were used to identify the modal prosperities resulted in very similar outcome in comparison to the other techniques considered. It was however noted that at times it was not possible to fit a reliable circle to the FRF data. Also, the weak and coupled modes were among the most difficult ones to analyze. He concluded that the circle-fit method could provide reliable results so long as there are enough data points around the resonance and that damping is not too low. On the other hand, it was stated that the method should not be used when the data contains noise around the resonance. He found that the global MDOF identification method could produce more consistent set of modal properties and is much faster rate than the SDOF approach.

In another paper, Fahey and Pratt (1998a) also explained the use of SDOF and MDOF techniques for fitting the experimental data. The SDOF techniques used were the Half-Power and Finite Difference method. They stated that the aforementioned techniques would be suitable when performing quick field analysis or when wanting to provide initial estimates of the parameters for use in the more complex MDOF techniques. As for the MDOF techniques they considered the simultaneous frequency-domain method and the rational polynomial method. They also addressed the topic of refitting the data for evaluating the global modal parameters. But in another article (1998b), they compared different time-domain modal estimation techniques.

Iglesias (2000) reported the comparison of the Half Power Frequency Domain Method, the Hilbert Transform Method and the Half Power Frequency Domain Method based on the so-called "zoom" measurements. It was concluded that third method was time consuming and that it should be used only when it is absolutely necessary to improve the frequency resolution. It was also stated that for light damping the Hilbert Transform would give better results than the Half Power Frequency Domain Method. Moreover, the first method was shown to have produced better fast loss factor with faster calculation speed in cases where coherence was good with small frequency resolution.

In another study, Naghipour *et al*. (2005) used different methods based on SDOF to evaluate vibration damping of Glass fiber reinforced plastic (GRP) glulam composite cantilever beams. The GRP used to reinforce the beams had various lay ups. They showed that damping coefficient based on the SDOF methodologies could be obtained with reasonable accuracy.

Yang (2003) used EMD for system identification of four degrees of freedom mechanical system, and evaluated the natural frequencies and damping of an *in-situ* tall building. Based on an experimental investigation, Xu and Chen (2004) also used EMD for damage detection of a three story shear-walled building. He concluded that damage location could be identified by the spatial distribution of the spikes (spikes in the curve of the sensor's quantity, i.e., voltage versus time), in the vicinity of the damage location in a building.

This paper outlines the details of six techniques used for determining the damping of a PVC material used in a pipe, based on time, frequency, and time-frequency domain methodologies. The methods considered in the time domain were Logarithmic Decrement Algorithm (LDA) and the Hilbert Transform Analysis (HTA). The method considered in the time-frequency domain was Hilbert-Huang spectral analysis based on Empirical Mode Decomposition (EMD). In the frequency method, the Moving Block Analysis (MBA), the Half Power Bandwidth (HPB), and the Circle fitting method were considered. The first two and the fourth methods were also used by Smith and Wereley (1997) for evaluation of damping ratio of composite rotorcraft flex beams reinforced with viscoelastic damping layers. For this, a PVC pipe with the length of 1531 mm and 159.1 mm outer diameter and wall-thickness of 4.55 mm was considered. The pipe was then instrumented using piezoelectric sensors and tested, and their damping ratios were evaluated using the above-mentioned methods. Five piezoelectric sensors were mounted at different locations along the length of the pipes and the pipe was subjected to an induced displacement and vibrational data was collected.

The other main objectives of our investigation are as follows

- To validate the Hilbert-Huang spectral analysis approach and its formulation for system identification by comparing the results obtained from this method to those of other commonly used methods. The integrity of the formulation was verified by considering the vibration characteristics of a multi degree of freedom system. These results would also be compared with the results produced by other workers based on a single degree of freedom system.
- To evaluate the influence of the location of the piezoelectric sensors used for gathering data on the resulting damping ratios.
- To compare the results obtained based on the three different approaches (i.e., the time domain, frequency domain and time-frequency domain).

Based on our findings, discussions will be provided outlining the strengths and shortfalls of the approaches.

To the best of our knowledge, the comparison of the methods considered within this work has not been reported in literature. Moreover, this is the first time that the Empirical Mode Decomposition (EMD) method has been applied to evaluate structural damping based on the data obtained from piezoelectric sensors.

## 2. Modeling and formulation of piezoelectric material

Various finite element formulations have been presented by several researchers for the assessment of dynamic response of piezoelectric materials. For instance, Tzou and Tseng (1990), and Rao and Sunar (1994) used the following equations to represent the dynamic response

$$\begin{aligned} [M]\{\ddot{u}\} + [K_{uu}]\{u\} + [K_{u\phi}]\{\phi\} &= \{F\} \\ [K_{\phi u}]\{u\} + [K_{\phi\phi}]\{\phi\} &= \{Q\} \end{aligned} \tag{1}$$

where

$[M] = \int_V \rho [N_u]^T [N_u] dV$ is the kinematically consistent mass matrix;

$[K_{uu}] = \int_V [B_u]^T [C^E][B_u] dV$ is the elastic stiffness matrix;

$[K_{u\phi}] = \int_V [B_u]^T [e]^T [B_\phi] dV$ is the piezoelectric coupling matrix;

$[K_{\phi\phi}] = -\int_V [B_\phi]^T [\varepsilon][B_\phi] dV$ is the dielectric stiffness matrix;

$\{F\} = \int_V [N_u]^T \{f_b\} dV + \int_{S_1} [N_u]^T \{f_S\} d\Omega + [N_u]^T \{f_c\}$ is the mechanical force vector, and

$\{Q\} = -\int_{S_2} [N_\phi]^T q_s d\Omega - [N_\phi]^T q_c$ is the electrical force vector.

In the above equations, $[M]$ is the mass matrix, $u$ is the displacement, $\phi$ is the electric potential, $Q$ is the applied concentrated electric charges, $\rho$ is the mass density, $[B_u]$ and $[B_\phi]$ are the derivatives of the shape functions, $[N_u]$ and $[N_\phi]$; $[C^E]$, $[\varepsilon]$, and $[e]$ are the elasticity, dielectric, and piezoelectric matrices respectively; $f_b$ denotes the body force, $f_s$ is the surface force, $f_c$ is the concentrated force, $q_s$ is the surface charge, $q_c$ is the point charge, $S_1$ is the region to which the surface forces are applied, and $S_2$ is the region where the electrical charges are applied. The above equations are presented in a partitioned form to reflect the coupling between the elastic and electric fields. Eq. (1) can be condensed to represent the sensor's potential in terms of the sensor displacement in the form

$$\{\phi_s\} = [K_{\phi\phi}]^{-1}(-[K_{u\phi}^T]\{u\}) \tag{2}$$

## 3. Experimental procedure and set up

### 3.1 Test setup and instrumentation

The test specimens used to determine the damping ratios were pipes made of PVC. A PVC pipe was instrumented by five piezoelectric sensors, as shown in Fig. 1. These sensors were bonded to the surface of the pipes using a West System's two-part epoxy. Once the sensors were bonded, they were held in place for eight hours under 20" of mercury vacuum to remove air voids and to ensure a strong bond. The pipes were held by a rigid metallic collar fastened to a massive steel platform. The material properties of the PVC pipe and piezoelectric patches are tabulated in Table 1.

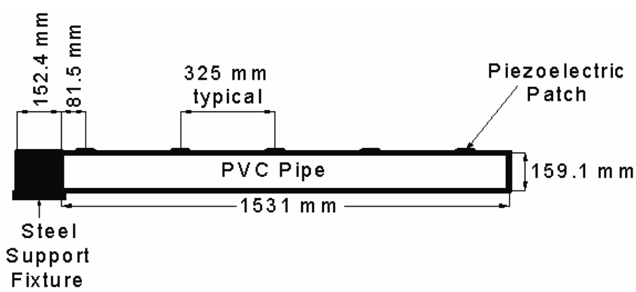


Fig. 1 Schematic of test setup

Table 1 Basic properties of the materials

| | |
|---|---|
| $E$ | 2800 MPa |
| $\nu$ | 0.35 |
| $\rho$ | 1150 kg/m$^3$ |
| Piezoelectric Patches | |
| $E$ | 69000 MPa |
| $\nu$ | 0.35 |
| $d_{31}$ | −179E-12 m/V |
| $K_3^T$ | 1800 |
| $\rho$ | 7700 kg/m$^3$ |

### *3.2 Test procedure*

As stated, the pipes were held in place as a cantilever beam. The rigid metallic collar was then secured in place under a 500 lb force using a 440,000 lb capacity Tinus-Olsen Universal Testing machine. Loading of the specimen was performed by hanging a known mass from a plastic strap on its free end, thus displacing the pipe's free end by a predetermined value. The strap was then cut, and the resulting vibration was monitored by the five piezoelectric patches.

The responses of the piezoelectric patches were simultaneously monitored with a differential channel set-up using a multi-purpose DT3010 data acquisition card manufactured by Data Translation (MA, USA). A C++ program was developed in-house to collect and process the data, using a sampling frequency of 1500 Hz.

## 4. Estimation of damping ratio using various methods of analysis

As stated, several methods of analysis, based on the time, frequency, and time-frequency domains were considered in our investigation. The following sections provide the details of each methodology.

### *4.1 Evaluation of damping ratio by the logarithmic decrement analysis (LDA)*

The true damping characteristic of a typical structural system is quite complex and rather difficult to define. However, it is a common practice to express the damping of a real system in terms of an equivalent viscous-damping ratio, $\xi$, which exhibits a similar decay rate under free-vibration condition. Consider any two successive positive peak amplitudes $v_n$ and $v_{n+1}$, occurring at times $n(2\pi/\omega_D)$ and $(n+1)(2\pi/\omega_D)$, respectively. For a critically damped system, the ratio of these two successive values can be represented by

$$\frac{v_n}{v_{n+1}} = \exp\left(\frac{2\pi\xi\omega}{\omega_D}\right) \tag{3}$$

where $\omega$ is the natural frequency, and subscript $D$ indicates the damped condition.

Taking the natural logarithm (ln) of both sides of the above equation and substituting $\omega_D = \omega\sqrt{1-\xi^2}$, one obtains the so-called "logarithmic decrement" of damping, $\delta$, by

$$\delta = \ln\frac{v_n}{v_{n+1}} = \frac{2\pi\xi}{\sqrt{1-\xi^2}} \tag{4}$$

The logarithm of the ratio of the amplitude of two oscillations that are $n$ cycles apart from each other, on the decaying transient of a single degree freedom system is defined by

$$\ln\frac{v_m}{v_{n+m}} = \frac{2n\pi\xi}{\sqrt{1-\xi^2}} \tag{5}$$

where the peak amplitude of the $m$th cycle and that of the $n$th cycles apart from it can be calculated by the transient signal of an under critically-damped system equation

$$v(t) = e^{-\xi\omega_n t}\sin(\sqrt{1-\xi^2}\,\omega_n t + \beta) \tag{6}$$

For low values of damping, Eq. (3) can be simplified to

$$\delta \doteq 2\pi n\xi \tag{7}$$

The damping ratio can thus be determined from the slope of the best-fitted line to the natural logarithm of each peak magnitude. Mathematically, the slope is equal to $-\xi\omega_n$.

Here we use output results of the piezoelectric sensors, which would be voltage versus time instead of using the usual displacement-time result. Typical output results of the piezoelectric sensors #1 and #5 are illustrated in Figs. 2(a), (b), and the data sensors #2, #3, and #4 was processed by the LDA methods, as illustrated in Figs. 3(a), (b), (c).

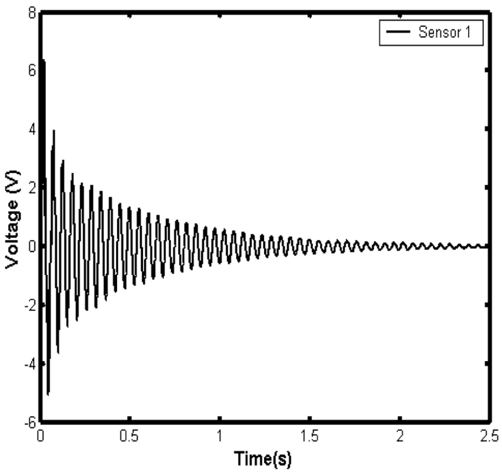


(a)

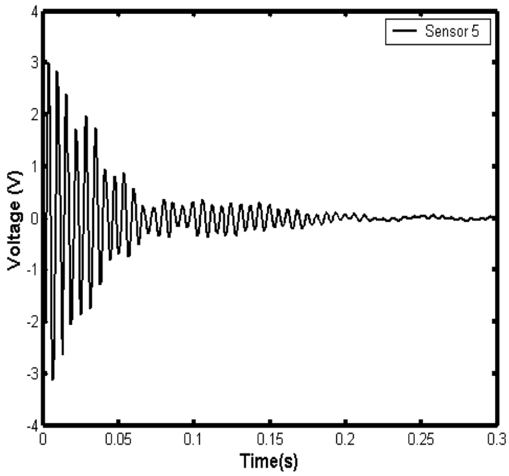


(b)

Fig. 2 Typical responses obtained from the sensors, (a) Sensor #1 (b) Sensor #5

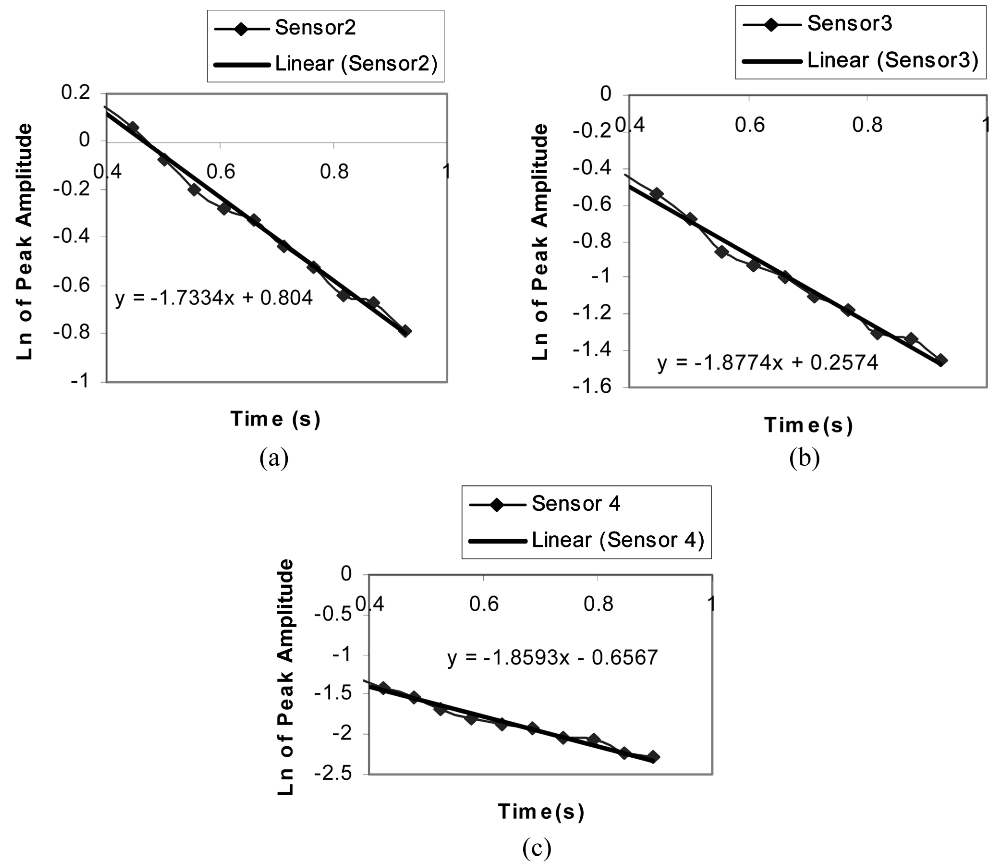


Fig. 3 Results obtained from the LDA method (a) Sensor # 2, (b) Sensor # 3, (c) Sensor # 4

### *4.2 Evaluation of damping ratio by the Hilbert transform analysis (HTA)*

The Hilbert transforms are linear operators that can be defined for a time domain, $x(t)$, by a convolution integral (Bracewell 1999)

$$y(t) = \frac{1}{\pi}\int_{-\infty}^{\infty}\delta(\tau)\frac{x(\tau)}{(t-\tau)}d\tau \quad \text{where} \begin{cases} \delta = -1 & \text{for} \quad \tau < 0 \\ \delta = 0 & \text{for} \quad \tau = 0 \\ \delta = +1 & \text{for} \quad \tau > 0 \end{cases} \tag{8}$$

The Hilbert transforms computes the so-called discrete-time analytic signal $x = x_r + ix_i$ such that $x_i$ is the Hilbert transform of the real vector $x_r$.

For a discrete-time analytic signal $x$, the last half of FFT($x$) is zero, and the first (DC) and center (Nyquist) elements of FFT($x$) are purely real. Moreover, an analytical signal represented by $[z(t) = x(t) + iy(t) = A(t)e^{i\theta(t)}]$, consists of a real part (the original data) and an imaginary part (the Hilbert transform portion). One of the most useful properties of this transformation scheme relative to the Fourier transform is that when $x(t)$ passes through the Hilbert Transformation, it leaves the magnitude of $X(f)$ unchanged (where $X(f)$ is the Fast Fourier transform of $x(t)$), but

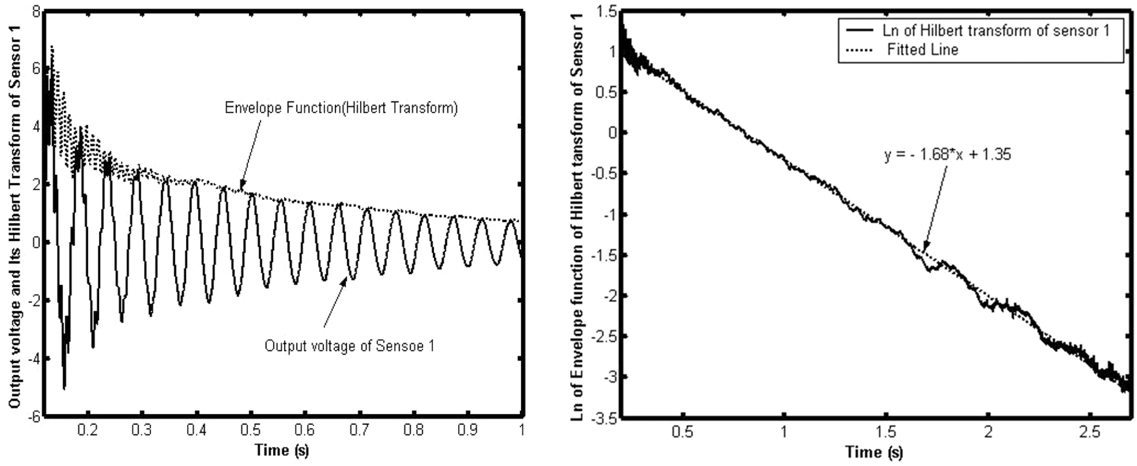


(a) (b)

Fig. 4 (a) Output voltage of Sensor #1 with its Envelope Function based on Hilbert transform, (b) plot of ln of Hilbert transform vs. time for data of sensor #1

rotates the phase angle by $\pi/2$. The Hilbert transform is therefore useful in calculating the instantaneous of a time domain, especially the amplitude and frequency.

Based on the above introductory background, the damping analysis can be performed by calculating the envelope signals for the transient output data of the piezoelectric sensors using the Hilbert transformation. This method was also applied by Smith and Wereley (1997) to evaluate the damping properties of a composite beam. For the transient response of a typical viscously damped system, the envelope signal, $A(t)$, and the instantaneous damping ratio $\xi(t)$ can be expressed by

$$A(t) = e^{-\xi\omega_n t} \quad \text{and} \quad \xi(t) = -\frac{d(\ln A(t))}{\omega_n dt} = \xi \tag{9}$$

A line can therefore be fitted through the logarithm of the envelope, and the slope of this line, $-\xi\omega_n$, would be equivalent to the damping ratio. Typical results of the HHT method for sensor #1 is illustrated in Figs. 4(a), (b).

### 4.3 Mathematical description of HHT

The Hilbert-Huang Transform (HHT) method was proposed by Huang *et al*. (1998). It consists of two parts: (i) the Empirical Mode Decomposition (EMD), and (ii) the Hilbert Spectral Analysis. With EMD, any complicated data set can be decomposed into a finite and often a smaller number of intrinsic mode functions.

The method is based on decomposing a signal into intrinsic mode functions (IMFs) using the empirical mode decomposition (EMD) method, where each IMF admits a well-behaved Hilbert transform. Then, the Hilbert transform is applied to each intrinsic mode function to obtain a decomposition of the signal in the frequency-time domain. This approach is also referred to as the Hilbert-Huang spectral analysis (HHSA) and it is applicable to any non-stationary signal (Huang *et al*. 1998, 1999). In this paper, the EMD method proposed by Huang (1998) and Huang *et al*. (1999), and will be used to decompose the measured response signal (output voltage of the piezoelectric sensors) into IMFs that would admit a well-behaved Hilbert transform. Based on the EMD, the modal response of each mode can be extracted from output voltage of a piezoelectric sensor.

The EMD procedure involves construction of the upper and lower envelopes of the signal by spline fitting, and then the average of both envelopes is computed. Then, the signal is subtracted from the mean. This process is referred to as the "sifting" process. The sifting process is repeated until the resulting signal becomes a monocomponent. The resulting monocomponent signal admits a well-behaved Hilbert transform; it is therefore referred to as an IMF. The original signal is then subtracted from IMF, and the repeated sifting process is applied to the remaining signals to obtain other IMFs. The process is iterated until m IMFs are obtained. The IMFs extracted from the sifting process may contain more than one frequency, which may not be the modal response of the output signal. During the sifting process in EMD, one can also impose an intermittency frequency, denoted by $\omega_{iut}$ so that the resulting IMF will not contain any frequency components smaller than $\omega_{iut}$. This is accomplished by removing data that have frequencies lower than $\omega_{iut}$, from the IMF by a straightforward counting process. This process was also implemented in the EMD procedures used by several other (Huang *et al*. 1998, 1999).

A code produced in MATLAB language was developed for carrying out the EMD procedure for the output voltages of the piezoelectric sensors.

### *4.4 Band-pass filtering and EMD*

The isolation of modal responses using the EMD method presented above has an advantage in that the frequency content of the signal at each time instant can be presented. However, the numerical computation based on this approach may be quite involved, in particular when the modal frequencies are high, and/or when the signal is polluted by an elevated noise level. In these cases, in order to obtain accurate modal responses, one should increase the number of siftings in the EMD. To simplify and decrease the computational efforts, an alternative approach based on the band-pass filter method was proposed by Yang *et al.* (2003). With Yang *et al.*'s proposed method, one can determine the approximate frequency range for each natural frequency from the Fourier spectrum of the output voltage. For example, if one considers the power spectrum analysis of sensor 1, as illustrated in Fig. 7(a), one would sees that the first mode is between 18 to 20 Hz. Each signal is then processed through the band-pass filters with a set frequency band. The time history obtained from the $j$th band-pass filter ($j$th natural frequency) is then processed through EMD. In this way, the first resulting IMF would be quite close to the $j$th modal response. By repeating the above procedure for the other natural frequencies, one can then obtain $n$ modal responses.

### *4.5 Evaluation of damping ratio by Hilbert-Huang spectral analysis (HHSA)*

The equation of motion for an $n$-DOF structure can be expressed by Yang *et al.* (2003)

$$M\ddot{X}(t) + C\dot{X}(t) + KX(t) = F(t) \tag{10}$$

in which $X(t) = [x_1, x_2, ..., x_n]$ represents the displacement vectors, $F(t)$ is the excitation vector and $M$, $C$ and $K$ are the $(n \times n)$ mass, damping, and stiffness matrices, respectively. With the assumption of the existence of normal modes, the displacement and acceleration responses can be decomposed into $n$ real modes

$$X(t) = \sum_{j=1}^{n} \phi_j Y_j(t); \quad \ddot{X}(t) = \sum_{j=1}^{n} \phi_j \ddot{Y}(t) \tag{11}$$

From the above equations, it is apparent that the $n \times n$ mode-shape matrix $\phi$ serves to transform the generalized coordinate vector $Y$ to the geometric coordinate vector $X$. The generalized components in vector $Y$ are called the "normal coordinates" of the structure.

By substituting Eq. (11) into Eq. (10) and using the orthogonal properties of the mode shapes, one can decouple Eq. (10) into $n$ modes

$$\ddot{Y}_j + 2\xi_j \omega_j \dot{Y} + \omega_j^2 Y = \phi_j^T F(t)/m_j \tag{12}$$

where $\omega_j$ is the $j$th modal frequency, $\xi_j$ is the $j$th modal damping ratio, and $m_j$ is the $j$th modal mass. Now, let's consider an impact load applied at the $p$th DOF (i.e., $f_p(t) = F_0\delta(t)$ and $f_j(t) = 0$ for all $j \neq p$ where $f_j(t)$ is the $j$th element of $F(t)$). Then, the acceleration response of the $j$th generalized modal co-ordinate is given by

$$\ddot{Y}_j(t) = \frac{F_0 \phi_{pj} \omega_j}{m_j \sqrt{1-\xi_j^2}} e^{-\xi_j \omega_j t} \cos\left(\omega_{dj} t + \varphi_j + \frac{\pi}{2}\right) \tag{13}$$

where $\phi_{pj}$ is the $p$th element of the $j$th modal vector $\phi_j$, $\omega_{dj} = \omega_j(1-\xi_j^2)^{0.5}$, is the $j$th damped modal frequency, and $\varphi_j = \tan^{-1}(2\xi_j\sqrt{1-\xi_j^2}/(1-2\xi_j^2))$ is the phase lag of the $j$th mode. The impulse acceleration response $\ddot{x}_k(t)$ of the structure at $k$ ($k = 1, ..., n$) DOF is given by

$$\ddot{x}_k(t) = \sum_{j=1}^{n} \phi_{kj} \ddot{Y}_j(t) = \sum_{j=1}^{n} \ddot{x}_{kj}(t) \tag{14}$$

where

$$\ddot{x}_{kj}(t) = \phi_{kj} \ddot{Y}_j(t) = B_{kj,p} e^{-\xi_j \omega_j t} \cos\left(\omega_{dj} t + \varphi_j + \frac{\pi}{2} + \varphi_{kj,p}\right) \tag{15}$$

in which

$$B_{kj,p} = \frac{F_0 |\phi_{kj}| |\phi_{pj}| \omega_j}{m_j \sqrt{1-\xi_j^2}} \tag{16}$$

$$x_{kj}(t) = B_{kj,p} \frac{e^{-\xi_j \omega_j t}}{(\xi_j^2 \omega_j^2 + \omega_{dj}^2)^2} * \begin{bmatrix} \xi_j^2 \omega_j^2 \sin\left(\omega_{dj} t + \varphi_j + \frac{\pi}{2} + \varphi_{kj,p}\right) + \\ 2\xi_j \omega_j \omega_{dj} \cos\left(\omega_{dj} t + \varphi_j + \frac{\pi}{2} + \varphi_{kj,p}\right) - \varpi_{dj}^2 \sin\left(\omega_{dj} t + \varphi_j + \frac{\pi}{2} + \varphi_{kj,p}\right) \end{bmatrix} \tag{17}$$

$$x_{kj}(t) = B_{kj,p} \frac{e^{-\xi_j \omega_j t}}{(\xi_j^2 \omega_j^2 + \omega_{dj}^2)^2} * \left[\sqrt{(\xi_j^2 \omega_j^2 - \omega_{dj}^2)^2 + 4\xi_j^2 \omega_j^2 \omega_{dj}^2} \cos\left(\omega_{dj} t + \varphi_j + \frac{\pi}{2} + \varphi_{kj,p} - \theta\right)\right]$$

where

$$\theta = tg^{-1}\left(\frac{\xi_j^2\omega_j^2 - \omega_{dj}^2}{2\xi_j\omega_j\omega_{dj}}\right) \tag{18}$$

In Eqs. (15), (17), and (18), $\varphi_{kj,p}$ is the phase difference between the $k$th element and the $p$th element in the $j$th mode shape. With the existence of normal modes, all the mode shapes are real and hence $\varphi_{kj,p}$ is either $\pm 2m\pi$ or $\pm(2m+1)\pi$, where $m$ is an integer, i.e.

$$\varphi_{kj}/\varphi_{pj} > 0 \quad \text{when} \quad \varphi_{kj,p} = \pm 2m\pi$$

$$\varphi_{kj}/\varphi_{pj} < 0 \quad \text{when} \quad \varphi_{kj,p} = \pm(2m+1)\pi$$

The Hilbert transform $x_{kj}(t)$ in Eq. (18) can be obtained using the Bedrosian's theorem (Hahn 1996), as follows

$$\tilde{x}_{kj}(t) = \frac{F_0|\phi_{kj}||\phi_{pj}|\omega_j}{m_j\sqrt{1-\xi_j^2}}\frac{e^{-\xi_j\omega_j t}\left(\sqrt{(\xi_j^2\omega_j^2+\omega_{dj}^2)^2 + 4\xi_j^2\omega_j^2\omega_{dj}^2}\right)}{(\xi_j^2\omega_j^2 + \omega_{dj}^2)^2} * \\ \left[a_{LK,j}\sin\left(\omega_{dj}t + \varphi_j + \frac{\pi}{2} + \varphi_{kj,p} - \theta\right) + \tilde{a}_{HK,j}\cos\left(\omega_{dj}t + \varphi_j + \frac{\pi}{2} + \varphi_{kj,p} - \theta\right)\right] \tag{19}$$

where

$$a_{LK,j} = \frac{1}{\pi}\int_0^{\omega_{dj}}\frac{2\xi_j\omega_j}{\xi_j^2\omega_j^2 + \omega^2}\cos(\omega t)d\omega \tag{20}$$

$$\tilde{a}_{HK,j} = \frac{1}{\pi}\int_{\omega_{dj}}^{\infty}\frac{2\xi_j\omega_j}{\xi_j^2\omega_j^2 + \omega^2}\sin(\omega t)d\omega \tag{21}$$

The analytical signal $Z_{kj}(t)$ of the $j$th mode is given by

$$Z_{kj}(t) = x_{kj}(t) + i\tilde{x}_{kj}(t) = A_{kj}(t)e^{i\beta_{kj}(t)} \tag{22}$$

In which the instantaneous amplitude $A_{kj}(t)$ and instantaneous phase angle $\beta_{kj}(t)$ are represented by

$$A_{kj}(t) = B_{kj,p}\frac{\sqrt{(\xi_j^2\omega_j^2+\omega_{dj}^2)^2 + 4\xi_j^2\omega_j^2\omega_{dj}^2}}{(\xi_j^2\omega_j^2 + \omega_{dj}^2)^2}\left\{\begin{array}{l} e^{-2\xi_j\omega_j t}\cos^2\left(\omega_{dj}t + \varphi_j + \frac{\pi}{2} + \varphi_{kj,p} - \theta\right) + \\ \left[\begin{array}{l} a_{LK,j}(t)\sin\left(\omega_{dj}t + \varphi_j + \frac{\pi}{2} + \varphi_{kj,p} - \theta\right) + \\ \tilde{a}_{HK,j}(t)\cos\left(\omega_{dj}t + \varphi_j + \frac{\pi}{2} + \varphi_{kj,p} - \theta\right) \end{array}\right]^2 \end{array}\right\}^{1/2} \tag{23}$$

$$B_{kj}(t) = \tan^{-1}\left\{e^{\xi_j\omega_j t}\left[a_{LK,j}(t)\tan\left(\omega_{dj}t + \varphi_j + \frac{\pi}{2} + \varphi_{kj,p} - \theta\right) + \tilde{a}_{HK,j}(t)\right]\right\} \tag{24}$$

For a special case in which $\xi_j$ is very small (less than 10%) and $\omega_j$ is large, Eqs. (20) and (21) yield

$$a_{LK,j} \approx \frac{1}{\pi}\int_0^{\infty} \frac{2\xi_j\omega_j}{\xi_j^2\omega_j^2 + \omega^2}\cos(\omega t)d\omega = e^{\xi_j\omega_j t} \tag{25}$$

$$\tilde{a}_{HK,j} = \frac{1}{\pi}\int_{\omega_{dj}}^{\infty} \frac{2\xi_j\omega_j}{\xi_j^2\omega_j^2 + \omega^2}\sin(\omega t)d\omega \approx 0 \tag{26}$$

Thus, Eq. (19) becomes

$$\tilde{x}_{kj}(t) = \frac{F_0|\phi_{kj}||\phi_{pj}|\omega_j}{m_j\sqrt{1-\xi_j^2}} \frac{e^{-\xi_j\omega_j t}\left(\sqrt{(\xi_j^2\omega_j^2+\omega_{dj}^2)^2 + 4\xi_j^2\omega_j^2\omega_{dj}^2}\right)}{(\xi_j^2\omega_j^2 + \omega_{dj}^2)^2} * \sin\left(\omega_{dj}t + \varphi_j + \frac{\pi}{2} + \varphi_{kj,p} - \theta\right) \tag{27}$$

and the amplitude $A_{kj}(t)$ and phase angle $\beta_{kj}(t)$ in Eq. (22) are given by

$$A_{kj}(t) = \frac{F_0|\phi_{kj}||\phi_{pj}|\omega_j}{m_j\sqrt{1-\xi_j^2}} \frac{e^{-\xi_j\omega_j t}\left(\sqrt{(\xi_j^2\omega_j^2+\omega_{dj}^2)^2 + 4\xi_j^2\omega_j^2\omega_{dj}^2}\right)}{(\xi_j^2\omega_j^2 + \omega_{dj}^2)^2} \tag{28}$$

$$\beta_{kj}(t) = \omega_{dj}t + \varphi_j + \frac{\pi}{2} + \varphi_{kj,p} - \theta \tag{29}$$

From Eqs. (28) and (29), one can obtain

$$\ln A_{kj}(t) = -\xi_j\omega_j t + \ln\left(\frac{F_0|\phi_{kj}||\phi_{pj}|\omega_j}{m_j\sqrt{1-\xi_j^2}} \frac{\left(\sqrt{(\xi_j^2\omega_j^2+\omega_{dj}^2)^2 + 4\xi_j^2\omega_j^2\omega_{dj}^2}\right)}{(\xi_j^2\omega_j^2 + \omega_{dj}^2)^2}\right) \tag{30}$$

$$\omega_j(t) = d\beta_{kj}(t)/dt = \omega_{dj} \tag{31}$$

With the measured output voltage of piezoelectric sensors, the EMD method can be used to decompose each measurement signal into $n$ modal responses. Then, each modal response can be processed through the Hilbert transform to determine the signal's instantaneous amplitude and phase angle. Finally, the system identification can be conducted to evaluate the natural frequencies and damping ratios by the process as described below.

It should be noted that for the sake of generality, the formulation presented in the above was developed based on the displacement data; alternatively, the above formulation can be developed based on the data obtained from another type of sensor, such as accelerometers or strain gauges.

The advantage of the outlined approach used for evaluating the damping and natural frequency is that it is not sensitive to the choice of sensor used to collect the data. In principle, signals obtained through any suitable sensors can be used for evaluation of the parameters of interest. For instance, one can directly input the output voltage of a piezoelectric sensor in Eq. (29) to start the calculations. In this paper we have used the output voltage of piezoelectric sensors for evaluating the damping of a PVC pipe.

## 5. Evaluation of natural frequencies and damping ratios based on Hilbert-Huang spectral analysis (HHST)

As stated, the advantage of the HHST method is that one needs data from only a single sensor (in our case, from one piezoelectric sensor), in order to evaluate the frequencies $\omega_j$ and damping ratios $\xi_j$ for a structure with $j = 1, 2, \ldots, n$ DOF. The measured output voltage response of the piezoelectric sensor contains sufficient information about $\omega_j$ and $\xi_j$ $(j = 1, 2, \ldots, n)$. In the first step of the analysis, one should perform a quick Fourier analysis to find the approximate natural frequency of the system. One should then use the band pass filter to separate the modal response of the system from each other. The procedure is described as follows

- For a $\xi_j$ (less than 10%), it follows from Eq. (13) that the damped natural frequency $\omega_{dj}$ can be obtained from the slope of the plot of phase angle $\theta_{pj}(t)$ versus time, $t$, for which $-\xi_j\omega_j$ can be estimated from the slope of the plot of the decaying amplitude $\ln A_{pj}(t)$ versus time $t$, obtained from Eq. (30).
- For the general case in which $\xi_j$ is not small, $A_{pj}(t)$ and $\theta_{pj}(t)$ are obtained from Eqs. (28) and (29). In this case, both $\theta_{pj}(t)$ and $\ln A_{pj}(t)$ would not be a linear functions of time $t$. Theoretically, $\xi_j$ and $\omega_{dj}$ can be determined from the non-linear Eq. (28). However, examination of the numerical results of Eq. (28) would reveal that the variation of amplitude $A_{pj}(t)$ introduces an instantaneous frequency modulation. This frequency modulation is referred to as "intra-wave modulation" by Huang *et al.* (1998). It was shown that the amplitude variation could cause a frequency fluctuation around the mean value of a carrier frequency, but not a change of its mean value (Huang *et al.* 1998). Consequently, we propose the use of linear least-

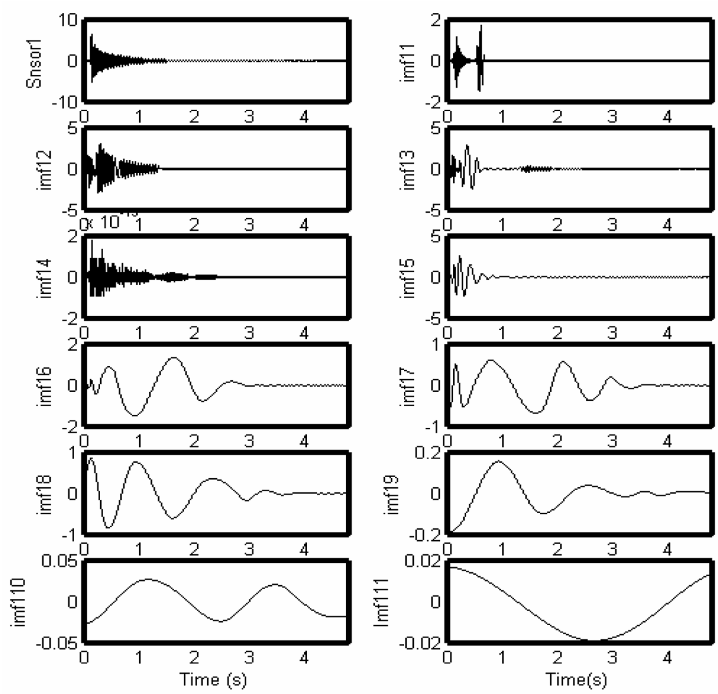


Fig. 5 Output voltage of sensor #1 and the intrinsic mode function (IMFs) plots

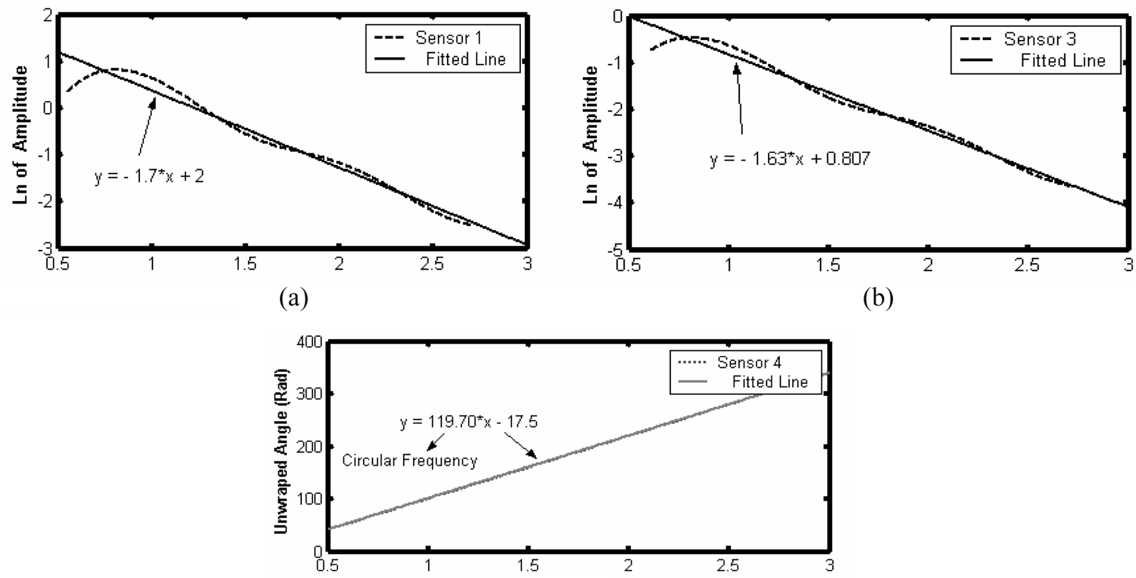


(a) (b)

(c)

Fig. 6 Application of the HHSA method on data obtained from (a) sensor #1, (b) sensor #3, and (c) #4

square fit procedures to estimate the mean values of the natural frequencies and damping ratios for general case.

Fig. 5 illustrates a typical sensor (output voltage of sensor #1) with its IMFs. As stated, one can determine the frequencies of the system from data obtained from any of the sensors. For the sake of illustration, the first natural frequency was derived from the date obtained from sensor # 4 (the slope of the curve) and illustrated in Fig. 6(c). It should be noted that alternatively the data from other sensors could have been used to produce the same frequency. Moreover, to demonstrate the strength of this method, the data obtained from sensors 1 and 3 are used to construct the curves of $\ln A_{pj}(t)$ versus $t$ (Figs. 6(a) and (b)). The damping ratio is extracted from the slope of the curves, which are shown to be very similar in values (see Table 3). Note that the numbers provide the percent damping ratios.

### *5.1 Evaluation of damping ratio by the moving block analysis (MBA)*

The Moving Block Analysis was introduced by Hammond and Doggett (1975), who investigated the response of a rotating model-scale rotor system. Tasker and Chopra (1990) showed that this method of damping analysis could be used to identify the stability characteristics of a high-level noise system. It was demonstrated that this method of analysis could effectively estimate the damping ratio for a variety of vibrating systems. This method was also used by Smith and Wereley (1997) for characterizing the dynamic response of a cantilevered composite beam hosting viscoelastic damping layers, excited by piezoelectric actuators.

In brief, the MBA is based on the calculation of the discrete approximation of the FFT of transient response data. This was presented by Tasker and Chopra (1990) in mathematical form as

$$X(\omega) = \sum_{r=0}^{N-1} x(r\Delta t)e^{-i\omega r\Delta t} \qquad T = N\Delta t \tag{32}$$

For a damped transient response, the above could be represented by

$$X(\omega, t_0) = \int_0^{T+t_0} Ae^{-\omega_n t}\sin(\sqrt{1-\xi^2}\,\omega_n t + \phi)e^{-i\omega t}dt \tag{33}$$

where $T$ is the block length and $t_0$ is the initial time of FFT.

Hammond and Doggett (1975) showed that the plot of the natural logarithm of the magnitude of FFT (i.e., $\ln|X(\omega_n, t)|$), versus time, would be the superposition of a straight line with a slope of $-\xi\omega_n$.

### 5.2 Determination of damping ratio using the half power bandwidth method

According to Richart *et al.* (1970), material damping ($\xi$) for each vibration mode can be determined from the respective resonant curve (see Fig. 8(a)), by means of the following expression

$$\frac{2\pi\xi}{\sqrt{1-\xi^2}} = \frac{\pi(f_2^2 - f_1^2)}{2\,f_m^2}\sqrt{\frac{A^2}{A_m^2 - A^2}}\frac{\sqrt{1-2\xi^2}}{1-\xi^2} \tag{34}$$

where $A_m$ is the maximum amplitude and $A$ is the amplitude at frequencies $f_1$ and $f_2$ at both sides of the resonant frequency $f_m$. For the case of a low damping ratio (less than 10%), Eq. (33) can be simplified to

$$\xi = A\frac{f_2^2 - f_1^2}{\sqrt{A^3 f_2^4 - 2A^2 f_2^2 f_1^2 + A^2 f_1^4 + 16 f_m^4 (A_m^2 - A^2)}} \tag{35}$$

Further simplification of Eq. (34) is obtained if the amplitude A is taken at $A_m/\sqrt{2}$ with the resonant curve being symmetric with respect to $f_m$

$$\xi = \frac{f_2 - f_1}{2f_m} \tag{36}$$

The above HPB formulation is one of the frequency domain methods usually admissible for materials that have small damping (Lanzan 1968). Karnopp *et al.* (2000) showed that when considering the plot of the frequency response function versus frequency, the bandwidth at point corresponding to $1/\sqrt{2}$ of the maximum amplitude would be approximately twice the product of the damping ratio and natural frequency. Some typical power spectrum results of the output voltage of some of the piezoelectric sensors # 1, 2, and 5 have been illustrated in Figs. 7(a), (b), (c).

### 5.3 Evaluation of damping ratio by the circle-fitting method

This method, first introduced by Kennedy and Pancu, uses the Argand plane to display the real and imaginary parts of the receptance frequency response function (FRF). In this manner, in the vicinity of each natural frequency, the FRF curve approaches a circle; the natural frequency can then be located at the point where the rate of change of the arc length of frequency attains a maximum. The model assumed that the damping is the hysteretic one and the damping factor could

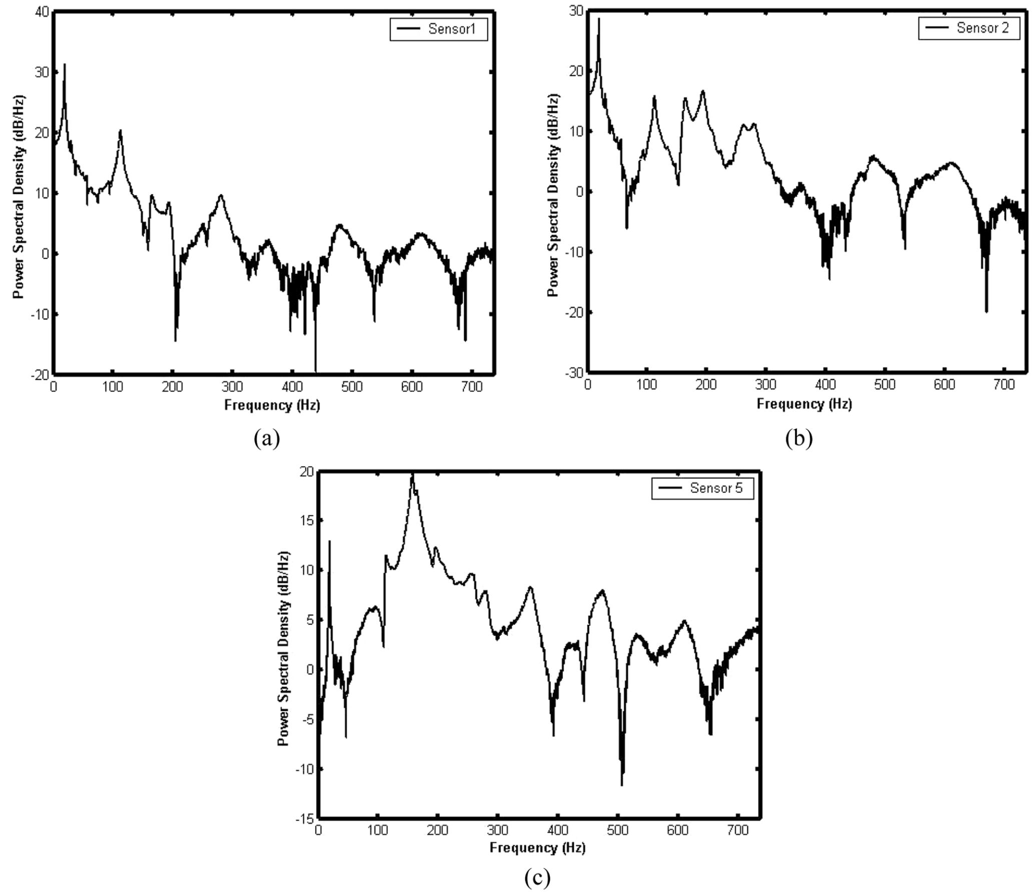


Fig. 7 Plot of power spectrum vs. frequency obtained from the output voltage of (a) sensor #1, (b) sensor #2, and (c) #5

be evaluated from a simplified half-power point calculation, and the mode shapes could be calculated from the ratios of the diameters of the circles fitted around each natural frequency for the various output response. In the present study, the circle-fitting method has been implemented as a mathematical solution, which accurately predicts the natural frequency $\omega_n$ and the damping factor $\eta$. Based on the vibration theory (Ewins 1984), the receptance FRF of an N degree of freedom system with hysteretic damping can be evaluated by the following equation

$$\alpha_{jk} = \sum_{r=1}^{N} \frac{C_{jk}^{r}}{\omega_r^2 - \omega^2 + i\eta_r\omega_r^2} \tag{37}$$

where $\eta_r$, $\omega_r$ and $C_{jk}^{r}$ are the hysteretic damping ratio, natural frequency, and complex constant, respectively, associated with each mode $r$. The Nyquist plot of $(\omega_r^2 - \omega^2 + i\eta_r\omega_r^2)^{-1}$ is a circle. Thus, multiplication by the complex constant $C_{jk}^{r}$ means a magnification or reduction of the circle radius, as well as giving a certain degree of rotation. In practice, the complex curve will not be exactly a circle around each natural frequency, but the curve will have circular arcs around those

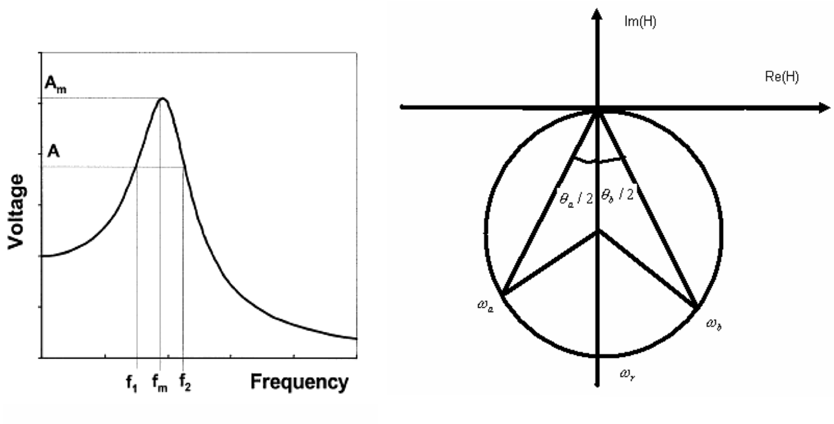


(a) (b)

Fig. 8 Schematics of the formation of the (a) HPB and (b) CFM methods

frequencies, especially when the modal frequencies are very similar.

The location and determination of the natural frequency are usually based on a frequency spacing technique. For a given mode, and apart from the effect of the complex modal constant, the phase angle $\theta_r$ associated with the dynamic response is given by Eq. (38) from which the resonant frequency $\omega_r$ can be extracted at a location where $d\omega^2/d\theta_r$ is a minimum. The phase angle can also be evaluated by

$$\theta_r = \tan^{-1}\left[\eta_r\left(1-\frac{\omega}{\omega_r}\right)^{-2}\right] \tag{38}$$

It is evident that calculating the minimum of $d\omega^2/d\gamma_r$ is equivalent to $d\omega^2/d\theta_r$. Thus, with reference to Fig. 8(b), by taking two points, *a* and *b* on the circle, one corresponding to a frequency slightly below the natural frequency ($\omega_b$), and the other corresponding to a frequency slightly above the natural frequency ($\omega_a$), one can express the damping factor $\eta_r$ by

$$\eta_r = \frac{\omega_a^2-\omega_b^2}{\omega_r^2}\frac{1}{\tan(\Delta\theta_a)+\tan(\Delta\theta_b)}, \quad \eta_r = 2\xi_r \tag{39}$$

An optimization program was developed for establishing the location of the centre of the circle. Fig. (9) illustrates the circles plotted based on the vibration data obtained through all piezoelectric sensors.

## 6. Finite element method for calculation of natural frequency of structure

To further verify the integrity of the approaches used here, a finite element analysis (FEA) was also conducted to evaluate the first two natural frequencies of the PVC pipes. In essence, the calculated damping ratio based on developed formula was used as an input for the finite element model. NISA finite element software (NISA 2004) was used for this task. The Solid 8-node element of NISA with 3 DOF per node (translational DOF) was used to model the pipes. NISA's solid 8-node piezoelectric element with 4 DOF per node (3 translational and one electric DOF ($\phi$ in Eq. (1))

was also used to model each piezoelectric patch. All displacements at the fixed end of the pipe were restricted in order to simulate the clamping of the pipe. The mesh that was used to model the pipe

Table 2 Natural frequency values obtained from the experimental and finite element analysis

| Bending mode | Natural frequency (Hz) (FEA) | Natural frequency HZ) experiment (FFT) | Natural frequency (Hz) experiment (EMD) |
|---|---|---|---|
| 1 | 19.01 | 19.07 | 19.05 |
| 2 | 109.17 | 112.7 | 111.3 |

(a)

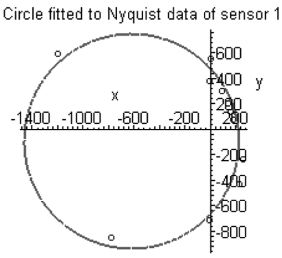


$\mathrm{Im}(x)^2 + \mathrm{Re}(x)^2 + 1242.04x + 227.19y - 305419.37 = 0$

$x_c = -621.02, y_c = -113.59, R = 839.04$

(b)

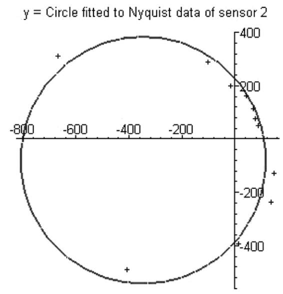


$\mathrm{Im}(x)^2 + \mathrm{Re}(x)^2 + 692.57x + 158.74y - 89376.27 = 0$

$x_c = -346.28, y_c = -79.37, R = 464.31$

(c)

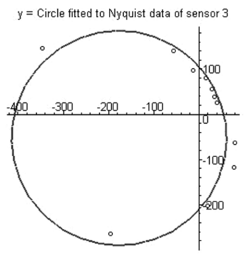


$\mathrm{Im}(x)^2 + \mathrm{Re}(x)^2 + 353.53x + 105.73y - 22621.28 = 0$

$x_c = -176.77, y_c = -52.86, R = 238.04$

(d)

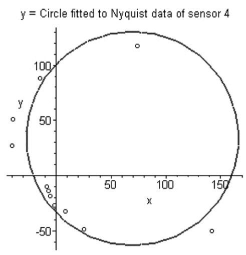


$\mathrm{Im}(x)^2 + \mathrm{Re}(x)^2 - 139.23x - 67.33y - 3446.05 = 0$

$x_c = 69.61, y_c = 33.67, R = 97.08$

(e)

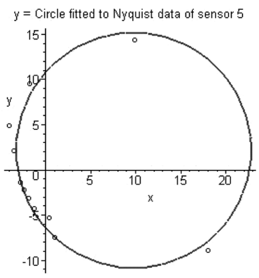


$\mathrm{Im}(x)^2 + \mathrm{Re}(x)^2 - 19.54x - 4.36y - 70.36 = 0$

$x_c = 9.77, y_c = 2.18, R = 13.06$

Fig. 9 The calculated results of the CFM for (a) Sensor #1, (b) Sensor #2, (c) Sensor 3, (d) Sensor #4, (e) Sensor #5 consisted of 242 elements in the axial direction and 80 in the circumferential direction, with 2 layers of elements through the thickness. Each piezoelectric patch was modeled with 8 × 4 × 1 piezo elements (length × width × thickness, respectively).

The Lanczos method was used for extracting the eigen-values of the system with a consistent mass formulation and a frontal solver. The results from the eigen-value and the Fast Fourier analysis are tabulated in Table 2.

## 7. Evaluation of the damping ratio and discussion of the results

As stated earlier, the main objective of this paper was to validate the Hilbert-Huang spectral analysis and formulation for system identification by comparing the results obtained from this method to those of other commonly used methods found in the literature.

Moreover, we also wanted to investigate the influence of location of the sensors on the dynamic response of the pipe. For this, we used the power spectrum method to establish the basic dynamic response of the pipe.

The mechanical material properties of the PVC pipe are tabulated in Table 1. The natural frequencies of the pipes were obtained based on the Fast Fourier analysis. The time history was collected using the five piezoelectric sensors. These results were considered as the time domain data for conducting the Fast Fourier analysis.

Table 3 Percent damping ratio evaluated based on the methods outlined

| Sensor number | LDA | HTA | HHT (EMD) | MBA | Circle fitted method | HPB |
|---|---|---|---|---|---|---|
| 1 | 1.47 | 1.39 | 1.42 | 1.36 | 1.37 | 1.86 |
| 2 | 1.55 | 1.36 | 1.38 | 1.32 | 1.27 | 1.86 |
| 3 | 1.56 | 1.33 | 1.35 | 1.25 | 1.22 | 1.86 |
| 4 | 1.55 | 1.30 | 1.32 | 1.22 | 1.21 | 1.94 |
| 5 | Not acceptable | .94 | 1.62 | .96 | 1.00 | 1.74 |

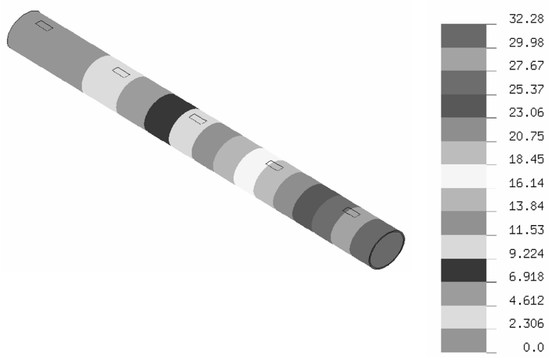


(a)

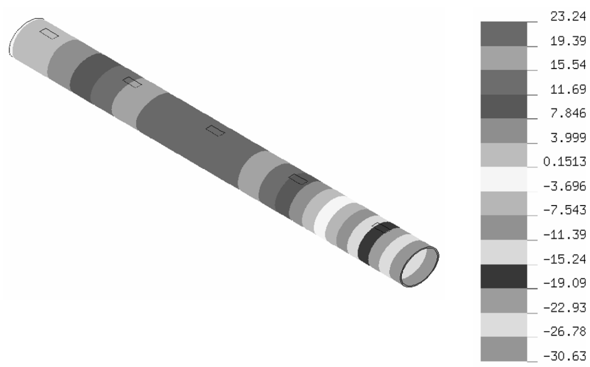


(b)

Fig. 10 Pipe's mode shapes determined by FEA (a) First mode, (b) Second Mode.

The natural frequencies of the pipes were calculated, by FEA, and by the EMD method. The FEA results are tabulated in Table 2. As can be seen, the experimental results are in good agreement with the FEA results. The first and second vibration mode shapes of the pipe are also illustrated in Figs. 10(a) and (b).

Moreover, using the LDA method, the natural logarithm of each peak (the absolute value of response obtained through each piezoelectric sensor) was calculated and plotted versus time (see Fig. (3)). A line was fitted through the resulting data using a least-mean-squares approach. The damping ratio was obtained through the slope of the best-fit line, as illustrated in Fig. (3). A summary of the results is tabulated in Table 3. A similar procedure was also followed for obtaining the damping ratio using the HTA, MBA, HPB, EMD and the circle-fitted methods, with the results also reported in Table 3. As it can be seen, all methods are capable of producing acceptable results, however, it is noted that the mixed time-frequency methods (i.e., HTA, EMD and MBA) could produce more consistent results than the other two methods. Therefore, the time-frequency domain approaches summarized above are recommended when evaluating the damping property of such damped materials.

Moreover, it is also noted that the results reported in the last row of Table 3 (i.e., the 5th sensor's results) are comparatively inconsistent with the results obtained form the other sensors. The data gathered through the 5th sensor exhibited some dual peaks in some of the first half cycles. This is believed to be due to the interference of loading induced high frequencies at the location of the sensor which was very close to the loading point.

## 8. Conclusions

Our experimental and analytical investigations considered two important dynamic issues governing the dynamic characteristics of plastic (PVC) pipes. Firstly, the integrity of five different admissible analytical methods for evaluating the damping ratio of plastic pipes was systematically examined both experimentally (through free vibration tests) as well as computationally (using finite element analysis). Secondly, the influence of the location of the piezoelectric sensors used for sensing the pipes' vibration was also investigated. Thirdly, the results obtained through the time domain analysis were compared to those obtained through the frequency domain methods.

An important aspect of the work presented here is the application of the Empirical Mode Decomposition (EMD) for evaluating the structural damping based on the data obtained from piezoelectric sensors.

The results clearly showed that the time domain results (i.e., the LDA method) obtained from the data from sensors positioned at various locations along the pipe's length were not consistent. It is believed that the discrepancy is due to the loading system used. It was also observed that some of the first half cycles in the response domain had dual peaks, which is believed to have occurred due to the nature of the applied loading and the adopted clamping mechanism. Nevertheless, results obtained through the frequency domain methods were found to be more consistent. Therefore, the frequency domain approaches summarized above are recommended when evaluating the damping property of such damped materials.

An important aspect of the work presented here is the development of the mathematical formulation based on the Empirical Mode Decomposition for calculating the damping coefficient and natural frequency of a multi-degree of freedom system based on the data obtained from a single piezoelectric sensor.

It is noted that although both pure time-domain method (i.e., LDA) and pure frequency-domain method (i.e., HPB) could produce consistent and acceptable results, it appears that the mixed time-frequency methods (i.e., HTA, EMD and MBA) produced more consistent results. Therefore, the time-frequency domain approaches summarized above are recommended when evaluating the damping property of such damped materials.

## Acknowledgements

The financial supports awarded by the Killam Foundation and NSERC, in the form of Doctoral Scholarships to the first and second authors, are gratefully acknowledged. We also acknowledge the support of the Atlantic Innovation Fund, awarded to the third author.

## References

Bracewell, R. (1999), *The Fourier Transform and Its Applications,* 3rd ed. McGraw-Hill, New York.

Ewins, D.J. (1984), *Modal Testing: Theory and Application*, Research Studies Press. New York.

Fahey, S. O'F and Pratt, J. (1998a), "Frequency domain modal estimation techniques", Experimental Techniques, 33-37, September/October.

Fahey, S. O'F. and Pratt, J. (1998b), "Time domain modal estimation techniques", Experimental Techniques, 45-49, November/December.

Hahn, S.J. (1996), "The Hilbert transform of the product $a(t)\ \cos(\omega_0 t + \phi_0)$", *Bulletin the Polish Academy Sci.*, **44**(1), 75-80.

Hammond, C.E. and Doggett, R.V. (1975), "Determination of subcritical damping by Moving-Block/Random applications", National Aeronautics and Space Administration Symposium on Flutter Testing Techniques, NASA **CP-415**, 59-76.

Huang, N.E., Shen, Z. and Long, S.R. (1999), "A new view of nonlinear water waves: The Hilbert spectrum", *Annual Review of Fluid Mechanics*, **31**, 417-457.

Huang, K. (1998), "A nondestructive instrument bridge safety inspection system (NIBSIS) using a transient load", US patent No. 09=210.693.

Huang, N.E., Shen, Z., Long, S.R., Wu, M.C., Shih, H.H., Zheng, Q., Yen, N.-C., Tung, C.C. and Liu, H.H. (1998), "The empirical mode decomposition and Hilbert spectrum for nonlinear and non-stationary time series analysis", *Proc. of the Royal Society of London—Series A*, **454**, 903-995.

Iglasias, A.M. (2000), *Investigating Various Modal Analysis Extraction Techniques to Estimate Damping Ratio.* Masters thesis, Department of Mechanical Engineering, Virginia Polytechnic Institute and State University, Blacksburg, Virginia.

Imregun, M. (1991), "A comparison of SDOF and Global MDOF modal analysis techniques when applied to a Lightly-damped linear structure", *Proc. of the Int. Modal Analysis Conf.*, 435-441.

Karnopp, D.C., Margolis, D.L. and Rosenberg, R.C. (2000), *System Dynamics: Modeling and Simulation of Mechatronic Systems*, Third Edition, John Wiley & Sons, Inc., Canada.

Lazan, B.J. (1968), *Damping of Materials and Members in Structural Mechanics*, Pergamon Press, Oxford, UK.

Naghipour, M., Zou, G.P. and Taheri, F. (2005), "Evaluation of vibration damping of GRP reinforced Glulam Composite Beams", *J. Eng. Mech.*, ASCE, in press.

NISA (2004), V.12, Engineering Mechanics Research Corporation, Troy, MI.

Rao, S.S. and Sunar, M. (1994), "Piezoelectricity and its use in disturbance sensoring and control of flexible structures: A survey", *Appl. Mech. Rev.*, **47**, 113-136.

Rayleigh, L. (1945), *Theory of Sounds* (two volumes). New York: Dover Publications, re-issue, second edition.

Richart, F.E. Jr., Hall, J.R. and Woods, R.D. (1970), *Vibration of Soils and Foundation*. Prentice-Hall, Inc., Englewood Cliffs, N. J.

Smith, C.B. and Wereley, N.M. (1997), "Composite rotorcraft flexbeams with viscoelastic damping layers for aeromechanical stability augmentation", Mechanics and Mechanisms of Material Damping, ASTM STP 1304, Wolfenden, A. and Kinra, V.K., Eds., 62-67.

Tasker, F.A. and Chopra, I. (1990), "Assessment of transient analysis techniques for rotor stability testing", *J. Am. Helicopter Soc.*, **35**(1), 39-50.

Tzou, H.S. and Tseng, C.I. (1990), "Distributed piezoelectric sensor/acyuatoractuator design for dynamic measurement/control of distributed parameter systems: A piezoelectric finite element approach", *J. Sound Vib.*, **138**(1), 17-34.

Xu Y.L. and Chen J. (2004), "Structural damage detection using empirical mode decomposition: Experimental investigation", *J. Eng. Mech.*, **130**, 1279-1288.

Yang, J.N., Lei, Y., Pan, S. and Huang, N. (2003), "System identification of linear structures based on Hilbert-Huang spectral analysis. Part 1: Normal modes", *Earthq. Eng. Struct. Dyn.*, **32**, 1443-1467.